International Journal of Innovative Computing, Information and Control
Volume **8**, Number **12**, December **2012**

 ISSN 1349-4198
pp. **8323–8340**

PERFORMANCE EVALUATION OF ACTIVE SYSTEMS USING THE NOVEL METHOD OF DESIGNING LARGER QUIET ZONES IN DIFFUSE FIELDS

Wen-Kung Tseng

Graduate Institute of Vehicle Engineering
National Changhua University of Education
No. 1, Jin-De Road, Changhua City 500, Taiwan
andy007@cc.ncue.edu.tw

Received September 2011; revised February 2012

Abstract. *This study evaluates the performance of quiet zones in broad-band diffuse fields using two and three channel systems. A novel method of designing zones of quiet has been proposed to obtain larger zones of quiet than are obtained with conventional methods. The principle of this new method is to maximize the area of the 10dB quiet zones over space and frequency in broad-band diffuse fields. This is in contrast to the conventional design methods, where the acoustic pressure is set to zero at given cancellation points, or the acoustic pressure is minimized over an area using 2-norm and ∞-norm strategies. It is shown that larger zones of quiet are obtained using this new method. A preliminary experiment has also been carried out to validate the simulation results. The main contributions of the paper are as follows. (1) A novel method of designing active systems to generate zones of quiet in broad-band diffuse fields is proposed. This novel method differs from the conventional method and previous works related to the active control of pure tone and broad-band diffuse fields. (2) Larger zones of quiet are obtained using the novel method proposed in this work compared to the results obtained in previous works. (3) This study analyzes quiet zones in broad-band diffuse fields through computer simulations and experiments. However, previous works have only performed computer simulations.*

Keywords: Quiet zones, Broad-band diffuse fields, A novel method, 2-norm, ∞-norm

1. **Introduction.** Previous studies of active noise control in free space have shown that the performance of the control system is largely dependent on the distance between primary sources and secondary sources or the secondary path fluctuation [1,2]. The most desirable noise control result would be the attenuation of sound pressure in all directions in space. Unfortunately, such global control can only be achieved when primary sources and control sources are located close to each other [3]. Nelson and Elliott examined an active control system with a pair of point sources on the basis of sound energy analysis [3]. They developed a set of matrix equations for a number of noise sources and control point sources located in a free space and discussed the principles of the global control of sound fields in great detail. Their work indicated that for the global control of noise, substantial reductions in total power output can be achieved only if the secondary sources are less than one half-wavelength away from the primary sources at the interest frequency. However, in practical applications the condition of maximal separation between primary and secondary sources may not always be satisfied. Under these circumstances, canceling the sound pressure in restricted regions and achieving quiet zones seem to be the only choice for achieving active noise control in free space. This control strategy is called local

control. Local active noise control can be applied inside automobiles and aircraft to cancel the noise near listeners' ears [4].

The conventional method is to generate a zone of quiet in pure tone diffuse fields to cancel the pressure at a point using a single secondary source [5-8]. The shape of the quiet zone created by using a single cancellation point and a monopole source is a shell-like volume surrounding the secondary source at low frequencies, and a smaller volume surrounding the cancellation point at higher frequencies [5]. The resulting on-axis pressure around the cancellation point is determined by the near field characteristics of the secondary source, which limit the diameter of the zone of quiet so that it is less than one tenth of a wavelength at the excitation frequency [6-8].

An alternative method of generating quiet zones in pure tone diffuse fields is to cancel the pressure or the pressure and particle velocity at a number of points using multi-pole secondary sources [9-13]. Canceling the pressure at several cancellation points could produce larger zones of quiet [9-11]; however, the optimal spacing between the cancellation points is dependent on the wavelength and therefore varies with frequency. Canceling the pressure and particle velocity has been shown to considerably increase the extension of the zone of quiet as compared with simply canceling the pressure [12-14].

All the approaches described above analyze quiet zones in pure tone diffuse fields which are produced by only a single frequency. Recent studies of broad-band diffuse fields have only concentrated on analysis of auto-correlation and cross-correlation of sound pressure [15-17]. However, there have also been some works related to controlling quiet zones in broad-band diffuse fields [18]. Therefore, this study takes a different approach by calculating a secondary field. First, the desired spatial extent of zone of quiet is defined. Then, a secondary field which maximizes the area of the 10dB quiet zone inside the desired quiet zone region over space and frequency is chosen. The results of computer simulations and experiments show that good attenuation in the desired quiet zones has been achieved using the proposed method. The quiet zones created by using the area maximization method of the 10dB quiet zone proposed in this paper are larger than those created by using the H_2 control method from a previous study [18]. This is because the two secondary monopoles in the area maximization method attempt to maximize the area of the 10dB quiet zone over space and frequency. Therefore, the amplitude of the secondary field is as close as possible to the 10dB reduction amplitude of the primary field with the opposite phase over the complete desired quiet zone. However, the H_2 control method minimizes the sum of the squared acoustic pressure over space and frequency [18]. Thus, the area maximization method can create larger quiet zones.

The remainder of this paper is organized as follows. In Section 2, the mathematical model of broad-band diffuse fields is derived. The novel method of designing quiet zones for a broad-band diffuse primary field is described in Section 3. The quiet zone simulations are presented in Section 4. The experiments are shown in Section 5. The paper is then concluded in Section 6.

2. **The Wave Model of Broad-band Diffuse Sound Fields.**

Previous studies have used the wave model, which is comprised of a large number of propagating waves arriving from various directions, to attain a pure tone diffuse field [5-8,13,14]. However, a wave model for broadband diffuse sound fields has not been derived. Therefore, for the sake of completeness, the mathematical derivation for broad-band diffuse fields is given below.

The diffuse field derived below is comprised of many propagating waves with random phases, arriving from uniformly distributed directions. Although the waves occupy a three-dimensional space, for the sake of simplicity, quiet zone analysis is performed over a two-dimensional area. Consider a single incident plane wave traveling along Line r

with its wave front parallel to Lines A and B as shown in Figure 1. We assume that the plane wave has some phase when approaching Line A, and has some phase shift due to the time delay when approaching Line B on the x-y plane. We now consider the plane perpendicular to Lines A and B and parallel to Line r, as illustrated in Figure 2. This incident plane wave has phase shift when approaching point (x_0, y_0) on Line B. The pressure at this point can therefore be expressed as

$$P(x_0, y_0, k) = (a + jb) \exp(-jkd), \tag{1}$$

where $a + jb$ account for the amplitude and phase of this incident plane wave when approaching Line A, k is the wave number and d is the additional distance traveled by the plane wave when approaching point (x_0, y_0) on Line B as shown in Figure 2.

The equation of Line A on the x-y plane can be written as

$$y = -x \tan(90^\circ - \varphi_L) = -x \cot \varphi_L. \tag{2}$$

The equation of Line B on the x-y plane can also be written as

$$y = -x \tan(90^\circ - \varphi_L) + m = -x \cot \varphi_L - m, \tag{3}$$

where m is the distance between Lines A and B on the y-axis.

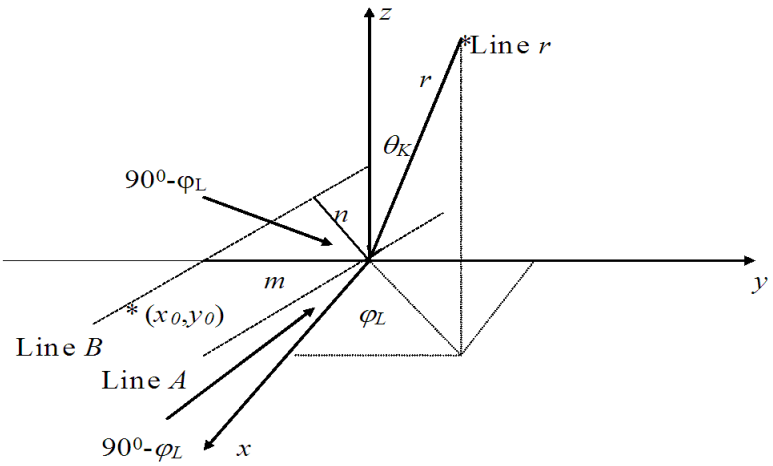

FIGURE 1. Definition of spherical co-ordinates r, θ, φ for an incident plane wave traveling along the direction of line r direction

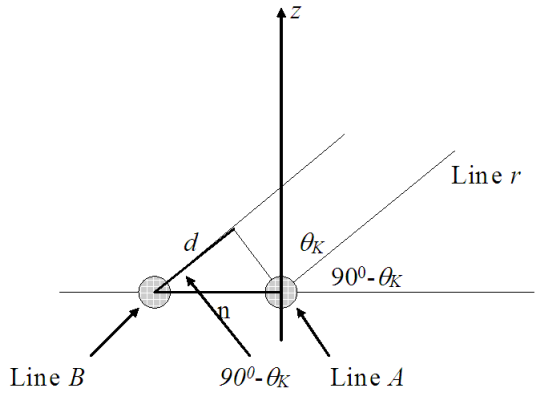

FIGURE 2. The plane perpendicular to lines A and B and parallel to line r

Substituting (x_0, y_0) into Equation (3) gives

$$m = -y_0 - x_0 \cot \varphi_L. \tag{4}$$

The distance n between Lines A and B as in Figure 1 can now be calculated as

$$n = m \cos(90^\circ - \varphi_L) = m \sin \varphi_L. \tag{5}$$

Substituting Equation (4) into Equation (5), the distance n becomes

$$n = -y_0 \sin \varphi_L - x_0 \cos \varphi_L. \tag{6}$$

The distance d in Figure 2 can now be calculated as

$$d = n \cos(90^\circ - \theta_K) = n \sin \theta_K. \tag{7}$$

Equation (6) can be substituted into Equation (7) and the distance d becomes

$$d = -y_0 \sin \theta_K \sin \varphi_L - x_0 \sin \theta_K \cos \varphi_L. \tag{8}$$

Therefore, Equation (1) can be written as

$$P(x_0, y_0, k) = (a + jb) \exp(jk(y_0 \sin \theta_K \sin \varphi_L + x_0 \sin \theta_K \cos \varphi_L)). \tag{9}$$

In our study, we chose 72 such incident plane waves together with random amplitudes and phases to generate an approximation of a diffuse sound field in order to coincide with results of previous works. Thus the diffuse sound field was generated by adding together the contributions of the 12 plane waves in the azimuthal directions (corresponding to azimuthal angles $\varphi_L = L \times 30^0$, $L = 1, 2, 3, \ldots, 12$) for each of the six vertical incident directions (corresponding to vertical angles $\theta_K = K \times 30^\circ$ for $K = 1, 2, 3, \ldots, 6$). The net pressure in the point (x_0, y_0) on the x-y plane due to the superposition of these 72 plane waves is then calculated from the expression

$$P_p(x_0, y_0, k) = \sum_{K=1}^{K\max} \sum_{L=1}^{L\max} (a_{KL} + jb_{KL}) \sin \theta_K \exp(jk(x_0 \sin \theta_K \cos \varphi_L + y_0 \sin \theta_K \sin \varphi_L)), \tag{10}$$

in which both the real and imaginary parts of the complex pressure are randomly distributed. The values of a_{KL} and b_{KL} are chosen from a random population with Gaussian distribution $N(0, 1)$. Moreover, the multiplicative factor $\sin \theta_K$ is included to ensure that, on average, the energy associated with the incident waves is uniform from all directions. Each set of 12 azimuthal plane waves arriving from a different vertical direction θ_K is distributed over a length of $2\pi r \sin \theta_K$, which is the circumference of the sphere defined by (r, φ, θ) for θ_K. This leads to higher density for waves with smaller θ_K, and thus more energy associated with small θ_K. To ensure uniform energy distribution, the amplitude of the waves is multiplied by $\sin \theta_K$, thus making the waves coming from the "dense" direction lower in amplitude. Substituting $k = \frac{2\pi}{c} f$ into Equation (10) gives

$$\begin{aligned} &P_p(x_0, y_0, f) \\ &= \sum_{K=1}^{K\max} \sum_{L=1}^{L\max} (a_{KL} + jb_{KL}) \sin \theta_K \exp\left(j \tfrac{2\pi}{c} f(x_0 \sin \theta_K \cos \varphi_L + y_0 \sin \theta_K \sin \varphi_L)\right), \end{aligned} \tag{11}$$

where f is frequency and c the speed of sound. Equation (11) is the wave model of the pure tone diffuse field. This is derived because only the single frequency plane wave arriving from the uniformly distributed directions is considered. If the diffuse field is broad-band

within the frequency range from *fl* to *fh*, then the wave model of the broad-band diffuse field P_{pb} can be expressed as

$$P_{pb}(x_0, y_0, f_{bn}) = \sum_{f_{bn}=fl}^{fh} \sum_{K=1}^{K\max} \sum_{L=1}^{L\max} (a_{KL}(f_{bn}) + jb_{KL}(f_{bn})) \sin\theta_K \exp(j\tfrac{2\pi}{c} f_{bn}(x_0 \sin\theta_K \cos\varphi_L + y_0 \sin\theta_K \sin\varphi_L)), \tag{12}$$

where f_{bn} is the frequency range from *fl* to *fh* Hz. Equation (12) is used for broad-band diffuse primary sound fields in this work. Next we describe the formulation of the control method, and how this method is used in the design of quiet zones in broad-band diffuse fields.

3. **Design of Quiet Zones in Broad-band Diffuse Fields.** This section presents a novel method of designing quiet zones in broad-band diffuse fields. The basic idea is to maximize the area of the 10dB quiet zone within the desired quiet zone over both space and frequency in broad-band diffuse fields. Figure 3 illustrates the configuration of the area maximization of the 10dB quiet zone over space and frequency. This study examines the case of a one-dimensional space and a broad-band diffuse primary field derived in Equation (12). In this case, the secondary sources are located at the origin and $(-0.05\text{m}, 0)$ point. A microphone can be placed at the desired zone of quiet or at other locations close to the secondary monopoles. The secondary sources are driven by feedback controllers connected to the microphone. The microphone detects the signal of the primary field, which is then filtered through the controllers to drive the secondary sources. The signals from the secondary sources are then used to maximize the area of the 10dB quiet zone at the desired quiet zone region.

The x-axis in Figure 3 is a one-dimensional spatial axis, which could be extended in principle, to 2 or 3D. The desired zone of quiet can be defined on this axis where a good attenuation is required. The y-axis is the frequency axis where the control bandwidth could be defined. The acoustic disturbance is assumed to be significant at the control frequency bandwidth. The shadowed region is the desired zone of quiet over space and frequency. The region to the right of the desired quiet zone region is the far field of the secondary sources. This region has a small control effort, and thus a small effect on the

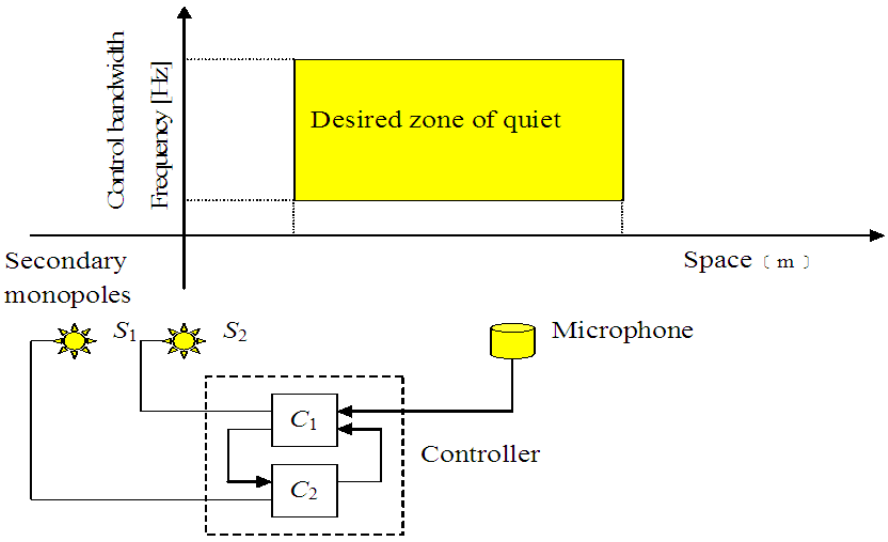

FIGURE 3. Configuration of the area maximization of the 10dB quiet zone over space and frequency with a two-channel feedback system

overall pressure of the active system. The region to the left of the desired quiet zone region is the near field of the secondary sources. The amplification of pressure might result in this region. To avoid significant pressure amplification, a pressure amplification constraint should be included in the design process using a constrained optimization. The regions above and below the desired quiet zone region represent frequencies outside the bandwidth. Due to the waterbed effect [19], a decrease in the disturbance at the control bandwidth will result in amplification outside the bandwidth. Therefore, pressure amplification outside the bandwidth must be constrained in the design process.

The feedback system used in this work can be applied to a practical active headrest system which includes primary and secondary loudspeakers, a microphone and a manikin head (listener) as shown in Figure 4. The microphone and the secondary loudspeakers are connected via feedback controllers. The active control system is designed to produce the zone of quiet around the listener's ear.

The feedback system can be configured using the internal model control [20] as shown in Figure 5, where P_1 is plant 1, the response between the input to the first secondary loudspeaker and the output of the microphone, P_{1o} is the internal model of plant 1, P_2 is plant 2, the response between the input to the second secondary loudspeaker and the output of the microphone, P_{2o} is the internal model of plant 2, P_{s1} and P_{s2} are the secondary fields at the field point away from the first and second secondary loudspeakers respectively, d is the disturbance of the broad-band diffuse field at the microphone location, d_s is the disturbance at the field point away from the microphone, and e is the error signal. In this work, it is assumed that P_{1o} is equal to P_1 and P_{2o} is equal to P_2. Therefore, the feedback system turns into a feedforward system with $x = d$, where x is the input to the control filters W_1 and W_2.

It is also assumed that the secondary and primary fields in both space and frequency are known. In addition, although a microphone is used for the feedback signal, pressure elsewhere is assumed to be known and this knowledge is used in the design process.

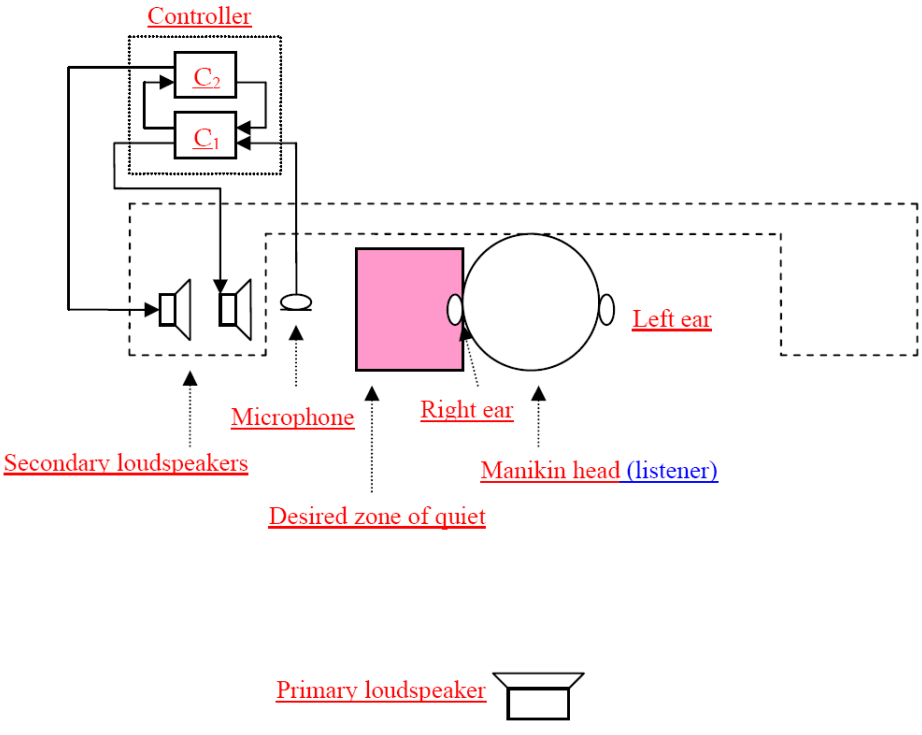

FIGURE 4. A practical active headrest system

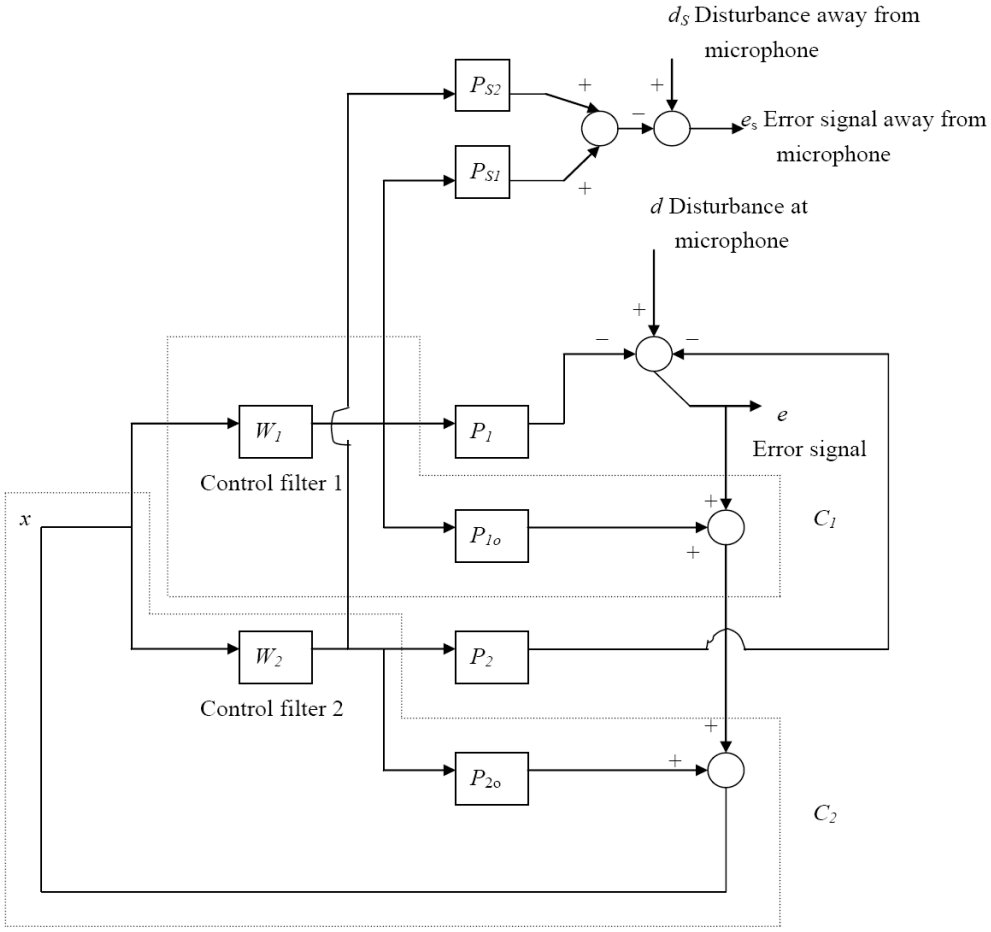

FIGURE 5. Two-channel feedback control system with two internal model controllers

Although it is not always practical to attain a good estimate of pressure far from the microphone, this still can be achieved in some cases using virtual microphone techniques which provide a sufficiently accurate estimate of acoustic pressure far from the microphone [15].

In order to simplify the simulations, the secondary loudspeakers are modeled as monopoles. Although monopole sources are not an accurate model for loudspeakers, it simplifies the secondary source modeling and assists in comparison between simulations and experiments. The secondary fields at the field point away from the secondary monopoles can be written as [9-11]:

$$P_{s1}(r_1, f) = \frac{A_1}{r_1} e^{-j2\pi f r_1/c} \tag{13}$$

$$P_{s2}(r_2, f) = \frac{A_2}{r_2} e^{-j2\pi f r_2/c} \tag{14}$$

where r_1 and r_2 are the distances from the field point to the first and second monopoles, respectively, A_1 and A_2 are the amplitude constants, f is the frequency and c is the speed of sound.

The plant responses can be written as:

$$P_1(r_{1o}, f) = \frac{A_{1o}}{r_{1o}} e^{-j2\pi f r_{1o}/c} \tag{15}$$

$$P_2(r_{2o}, f) = \frac{A_{2o}}{r_{2o}} e^{-j2\pi f r_{2o}/c} \tag{16}$$

where r_{1o} and r_{2o} are the distances from the microphone to the first and second monopoles, A_{1o} and A_{2o} are the amplitude constants. The error signal can be expressed as:

$$e_s(r,f) = d_s - dW_1P_{s1} - dW_2P_{s2} \tag{17}$$

The disturbance in this work is the broad-band diffuse field. Therefore, Equation (17) can also be expressed as:

$$e_s(r,f) = P_{pbs} - P_{pb}W_1\frac{A_1}{r_1}e^{-j2\pi fr_1/c} - P_{pb}W_2\frac{A_2}{r_2}e^{-j2\pi fr_2/c}, \tag{18}$$

where P_{pbs} is the broad-band diffuse primary field at the field points and P_{pb} is the broad-band diffuse field at the microphone. To achieve robust stability, the closed-loop of the feedback system must satisfy the following condition:

$$\left\| W_1B_1\frac{A_{1o}}{r_{1o}}e^{-j2\pi fr_{1o}/c} + W_2B_2\frac{A_{2o}}{r_{2o}}e^{-j2\pi fr_{2o}/c} \right\|_\infty < 1, \tag{19}$$

where B_1 and B_2 are the multiplicative plant uncertainty bounds for plants 1 and 2 and r_{1o} and r_{2o} are the distances from the microphone to the first and second monopoles, respectively. The terms $e^{-j2\pi fr_{1o}/c}$ and $e^{-j2\pi fr_{2o}/c}$ represent plant responses. Therefore, the robust stability condition $\|WPB\|_\infty < 1$ is followed. For the amplification limit, a constraint could be added to the optimization process as follows.

$$\left\| \left(1 - W_1\frac{A_1}{r_1}e^{-j2\pi fr_1/c} - W_2\frac{A_2}{r_2}e^{-j2\pi fr_2/c}\right) D \right\|_\infty < 1, \tag{20}$$

where $1/D$ is the desired enhancement bound.

In this work the control problem is formulated as a convex, nonlinear constrained optimization problem and the Sequential Quadratic Programming (SQP) method is used to solve the optimization problem [21,22]. In general the optimization problem can be defined as follows [21,22]:

$$\begin{array}{ll} \underset{\boldsymbol{x}}{\text{Minimize}} & f(\boldsymbol{x}) \\ \text{Subject to} & c_i(\boldsymbol{x}) = 0 \quad i = 1,\ldots,m_e \\ & c_i(\boldsymbol{x}) \le 0 \quad i = m_e+1,\ldots,m, \end{array} \tag{21}$$

where $f(\boldsymbol{x})$ is a nonlinear real scalar function of the optimization parameter vector $\boldsymbol{x} = [x_1,\ldots,x_n]^T$, and $c_i(\boldsymbol{x})$ are nonlinear scalar constraint functions, which can be written in a vector form as $\boldsymbol{c}(\boldsymbol{x}) = [c_1(\boldsymbol{x}),\ldots,c_m(\boldsymbol{x})]^T$. $c_i(\boldsymbol{x})$, $i = 1,\ldots,m_e$ are referred to as equality constraints, and $c_i(\boldsymbol{x})$, $i = m_e+1,\ldots,m$ are referred to as inequality constraints [21,22].

The optimal solution for the problem defined in Equation (21) must satisfy a set of equations, known as the Kuhn-Tucker equations [23]. The Kuhn-Tucker equations thus form a necessary condition for the optimality of a solution. Furthermore, when the optimization problem is convex, so that both the objective function f and the constraints c_i shown in Equation (21) are convex, the Kuhn-Tucker equations are also necessary to achieve sufficient conditions for the global minimum point. The Kuhn-Tucker equations are written below in terms of the Lagrangian function:

$$\nabla \boldsymbol{L}(\boldsymbol{x}^*, \boldsymbol{\lambda}^*) = 0 \tag{22}$$

$$c_i(\boldsymbol{x}^*) = 0 \quad i = 1,\ldots,m_e \tag{23}$$

$$c_i(\boldsymbol{x}^*) \le 0 \quad i = m_e+1,\ldots,m \tag{24}$$

$$\lambda_i^* c_i(\boldsymbol{x}^*) = 0 \quad i = 1,\ldots,m \tag{25}$$

$$\lambda_i^* \ge 0 \quad i = m_e+1,\ldots,m \tag{26}$$

where $\nabla \boldsymbol{L}$ is the first derivative of the Lagrangian function, and $\boldsymbol{L}(\boldsymbol{x}, \boldsymbol{\lambda})$ is the Lagrangian function which can be defined as $\boldsymbol{L}(\boldsymbol{x}, \boldsymbol{\lambda}) = f(\boldsymbol{x}) + \boldsymbol{\lambda}^T \boldsymbol{c}(\boldsymbol{x})$, where $\boldsymbol{\lambda} = [\boldsymbol{\lambda}_1, \ldots, \boldsymbol{\lambda}_n]$. The condition for a minimum point becomes $\nabla \boldsymbol{L}(\boldsymbol{x}^*, \boldsymbol{\lambda}^*) = 0$, where $\boldsymbol{\lambda}^*$ are the Lagrange multipliers associated with $\boldsymbol{x}^*$. $\boldsymbol{x}$ and $\boldsymbol{\lambda}$ at the solution point are denoted by $\boldsymbol{x}^*$ and $\boldsymbol{\lambda}^*$ respectively. These conditions do not hold if some regulatory assumptions (also called constraints qualifications) are not met [24], although this happens only in extreme cases. Equations (23) and (24) are simply re-statements of the constraints equations. Equation (25) is related to the fact that inactive constraints at the solution point have corresponding Lagrange multipliers of zero, which means that they do not affect the solution. Indeed, inactive constraints have no effect on the solution point if they are removed. Equation (26) states that all the Lagrange multipliers of the inequality constraints are non-negative, i.e., they are zero for the inactive inequality constraints and positive for the active inequality constraints. A more detailed description of the Kuhn-Tucker conditions can be found in previous studies [23,24].

In this work, the Sequential Quadratic Programming (SQP) method is used to solve the optimization problem. The nonlinear programming problem defined in Equation (21) can be solved iteratively by calculating the solution to a quadratic sub-problem at each iteration. The solution to the Quadratic Programming (QP) sub-problem gives the search direction for the next iteration. First, the formulation of the quadratic sub-problem will be described, and then the complete Sequential Quadratic Programming algorithm will be given. According to the Lagrangian function and the Kuhn-Tucker condition, as in Equation (22), the solution point is a stationary point of the Lagrangian function. This condition is written in a matrix form as follows:

$$\underline{\nabla} \boldsymbol{L}(\boldsymbol{x}^*, \boldsymbol{\lambda}^*) = 0 \tag{27}$$

where the operator $\underline{\nabla}$ is denoted to be gradient with respect to both $\boldsymbol{x}$ and $\boldsymbol{\lambda}$, i.e., $\underline{\nabla} = [\nabla_{\boldsymbol{x}} \ \nabla_{\boldsymbol{\lambda}}]^{\mathrm{T}}$.

Given a point $(\boldsymbol{x}_k, \boldsymbol{\lambda}_k)$, and by approximating the Lagrangian function with a quadratic function (using truncated Taylor series), an approximation to $(\boldsymbol{x}^*, \boldsymbol{\lambda}^*)$ can be found by minimizing the approximated quadratic function. A truncated Taylor series expansion is used to approximate Equation (27), for the point $(\boldsymbol{x}_k + \boldsymbol{\delta}_{\boldsymbol{x}}, \boldsymbol{\lambda}_k + \boldsymbol{\delta}_{\boldsymbol{\lambda}})$ around the point $(\boldsymbol{x}_k, \boldsymbol{\lambda}_k)$, as in the following equation:

$$\underline{\nabla} \boldsymbol{L}(\boldsymbol{x}_k + \boldsymbol{\delta}_{\boldsymbol{x}}, \boldsymbol{\lambda}_k + \boldsymbol{\delta}_{\boldsymbol{\lambda}}) \approx \underline{\nabla} \boldsymbol{L}(\boldsymbol{x}_k, \boldsymbol{\lambda}_k) + \underline{\nabla}^2 \boldsymbol{L}(\boldsymbol{x}_k, \boldsymbol{\lambda}_k)[\boldsymbol{\delta}_{\boldsymbol{x}} \ \boldsymbol{\delta}_{\boldsymbol{\lambda}}]^T \tag{28}$$

where $\underline{\nabla}^2$ is the Hessian matrix with respect to both $\boldsymbol{x}$ and $\boldsymbol{\lambda}$. It is required that the point $(\boldsymbol{x}_k + \boldsymbol{\delta}_{\boldsymbol{x}}, \boldsymbol{\lambda}_k + \boldsymbol{\delta}_{\boldsymbol{\lambda}})$ will approximate $(\boldsymbol{x}^*, \boldsymbol{\lambda}^*)$, and the left-hand side of Equation (28) is set to zero, which, according to the Kuhn-Tuker conditions, will occur at the solution point. Evaluating the right-hand side of Equation (28), after some manipulation [21], and setting

$$\boldsymbol{\lambda}_{k+1} = \boldsymbol{\lambda}_k + \boldsymbol{\delta}_{\boldsymbol{\lambda}}, \quad \boldsymbol{d}_k = \boldsymbol{\delta}_{\boldsymbol{x}}, \tag{29}$$

yields the results in the following equation, where only gradients with respect to $\boldsymbol{x}$ are included (for notational convenience, the condition of $\nabla_x = \nabla$ is required):

$$\begin{gathered} \underline{\nabla}^2 \boldsymbol{L}(\boldsymbol{x}_k, \boldsymbol{\lambda}_k) \boldsymbol{d}_k + \nabla \boldsymbol{c}(\boldsymbol{x}_k)^T \boldsymbol{\lambda}_{k+1} + \nabla f(\boldsymbol{x}_k) = 0 \\ \nabla \boldsymbol{c}(\boldsymbol{x}_k)^T \boldsymbol{d}_{k+1} + \boldsymbol{c}(\boldsymbol{x}_k) = 0 \end{gathered} \tag{30}$$

A quadratic function and linear constraints (i.e., a QP problem) are now defined in the following way:

$$\begin{array}{ll} \underset{\boldsymbol{d}_k}{\text{Minimize}} & \frac{1}{2} \boldsymbol{d}_k^T \nabla^2 \boldsymbol{L}(\boldsymbol{x}_k, \boldsymbol{\lambda}_k) \boldsymbol{d}_k + \nabla f(\boldsymbol{x}_k)^T \boldsymbol{d}_k = 0 \\ \text{Subject to} & \nabla \boldsymbol{c}(\boldsymbol{x}_k)^T \boldsymbol{d}_k + \boldsymbol{c}(\boldsymbol{x}_k) = 0 \end{array} \tag{31}$$

Equation (30) corresponds to the Kuhn-Tucker condition in Equation (31), i.e., the gradient of the Lagrangian function is zero. This means that the solution to the QP problem in Equation (31), which produces $\boldsymbol{d}_k$ and the corresponding Lagrange multipliers $\boldsymbol{\lambda}_{k+1}$, gives an approximation of the solution point of the original nonlinear programming problem, i.e., $\boldsymbol{x}^* \approx \boldsymbol{x}_k + \boldsymbol{d}_k$, and $\boldsymbol{\lambda}^* = \boldsymbol{\lambda}_{k+1}$, where the approximation arises from the quadratic approximation of the Lagrangian function. Therefore, the quadratic sub-problem in Equation (31) can be used in an iterative procedure, where in each iteration the solution to the sub-problem gives a search direction $\boldsymbol{d}_k$ for the solution of the nonlinear problem, and an update of the Lagrange multipliers. For the following sub-problem, Equation (31) can be generalized to include inequality constraints [23], which correspond to the nonlinear optimization problem in Equation (21):

$$\begin{array}{ll} \underset{\boldsymbol{d}_k}{\text{Minimize}} & \frac{1}{2}\boldsymbol{d}_k^T \nabla^2 L(\boldsymbol{x}_k, \boldsymbol{\lambda}_k)\boldsymbol{d}_k + \nabla f(\boldsymbol{x}_k)^T \boldsymbol{d}_k = 0 \\ \text{Subject to} & \nabla c_i(\boldsymbol{x}_k)^T \boldsymbol{d}_k + c_i(\boldsymbol{x}_k) = 0 \quad i = 1, \ldots, m_e \\ & \nabla c_i(\boldsymbol{x}_k)^T \boldsymbol{d}_k + c_i(\boldsymbol{x}_k) \leq 0 \quad i = m_e + 1, \ldots, m \end{array} \tag{32}$$

The algorithm which solves the nonlinear programming problem using Sequential Quadratic Programming is outlined as follows:

SQP algorithm

(1) Set initial feasible point $\boldsymbol{x}_0$ and initial Lagrange multipliers $\boldsymbol{\lambda}_0$. Set $k = 0$.
(2) Check termination conditions for $\boldsymbol{x}_k$ or k.
(3) Update the estimate of the Hessian matrix $\underline{\nabla}^2 \boldsymbol{L}(\boldsymbol{x}_k, \boldsymbol{\lambda}_k)$ (the updating methods will be described later).
(4) Formulate and solve the quadratic sub-problem for iteration k, as in Equation (32). Find $\boldsymbol{\lambda}_{k+1}$ and $\boldsymbol{d}_k$.
(5) Perform a line search to find α that will produce sufficient decrease in the objective function of the original nonlinear problem at the point $\boldsymbol{x}_k + \alpha \boldsymbol{d}_k$ for $\alpha \in [0, 1]$.
(6) Update $\boldsymbol{x}_{k+1} = \boldsymbol{x}_k + \alpha \boldsymbol{d}_k$.
(7) Update $k = k + 1$ and return to stage (2).

In order to complete the discussion of the SQP algorithm, the updating of the Hessian matrix and the line search methods will be described. These are necessary because the Lagragian function is not quadratic for a general nonlinear problem, implying that (1) the Hessian matrix differs for different $\boldsymbol{x}_k$, and thus must be updated along the iterations, and (2) the solution $\boldsymbol{x}_k + \boldsymbol{d}_k$ of the QP sub-problem might not be close to the solution of the nonlinear problem since it is generally not quadratic. Thus, $\boldsymbol{d}_k$ is used only as a direction vector for the solution, and a suitable α is found so that the original objective function is significantly reduced. The method used for updating the Hessian matrix and for performing the line search can be expressed as follows ($\boldsymbol{H}_k$ denotes the Hessian matrix at iteration k):

$$\boldsymbol{H}_{k+1} = \boldsymbol{H}_k + \frac{\boldsymbol{q}_k \boldsymbol{q}_k^T}{\boldsymbol{q}_k^T \boldsymbol{s}_k} - \frac{\boldsymbol{H}_k^T \boldsymbol{H}_k}{\boldsymbol{s}_k^T \boldsymbol{H}_k \boldsymbol{s}} \tag{33}$$

where $\boldsymbol{s}_k = \boldsymbol{x}_{k+1} - \boldsymbol{x}_k$, $\boldsymbol{q}_k = \nabla \boldsymbol{L}(\boldsymbol{x}_{k+1}, \boldsymbol{\lambda}_k) - \nabla \boldsymbol{L}(\boldsymbol{x}_k, \boldsymbol{\lambda}_k)$.

During the updating process, measures are taken (such as the modification of $\boldsymbol{q}_k$) to keep $\boldsymbol{H}_{k+1}$ positive, which ensures that the quadratic sub-problem will have a unique minimum. The line search is conducted to find an appropriate α such that a significant decrease in a merit function, which includes both the objective function and the constraints, is obtained. The merit function is described as:

$$\psi(\boldsymbol{x}) = f(\boldsymbol{x}) + \sum_{i=1}^{m_e} \sigma_i c_i(\boldsymbol{x}) + \sum_{i=m_e+1}^{m} \sigma_i \max\{0, c_i(\boldsymbol{x})\} \tag{34}$$

where violated constraints are used to penalize the merit function, and σ_i are used as the penalty coefficients.

The SQP method is used in this work to find the optimal solution of the control problem in a finite number of iterations. Commercially available software exists to solve SQP problems, such as the MATLAB *fmincon*() function [25]. Equation (21) mentioned above can be used in this work and can be rewritten as:

$$\begin{array}{ll} \underset{\boldsymbol{x}}{\text{Maximizing}} & -f(\boldsymbol{x}) \\ \text{Subject to} & c_i(\boldsymbol{x}) = 0 \quad i = 1, \ldots, m_e \\ & c_i(\boldsymbol{x}) \leq 0 \quad i = m_e + 1, \ldots, m \end{array} \tag{35}$$

The objectives of this study are to create larger 10dB quiet zones in broad-band diffuse fields and to achieve robust stability and amplification constraints. Therefore, a novel method of maximizing 10dB quiet zones in broad-band diffuse fields is proposed. The formulation of the method is given as follows.

$$\begin{array}{l} \text{Maximizing} \quad A \\ \text{Subject to} \\ \left\| 10\log_{10} \frac{|e_s(x,y,f)|^2}{\left|p_{pbs}(x,y,f)\right|^2} \right\|_\infty < -10\text{dB inside the area } A, \\ \left\| W_1 B_1 \frac{A_{1o}}{r_{1o}(x,y)} e^{-j2\pi f r_{1o}(x,y)/c} + W_2 B_2 \frac{A_{2o}}{r_{2o}(x,y)} e^{-j2\pi f r_{2o}(x,y)/c} \right\|_\infty < 1 \\ \left\| \left(1 - W_1 \frac{A_1}{r_1(x,y)} e^{-j2\pi f r_1(x,y)/c} - W_2 \frac{A_2}{r_2(x,y)} e^{-j2\pi f r_2(x,y)/c}\right) D \right\|_\infty < 1 \end{array} \tag{36}$$

where A is the area of the 10dB quiet zone inside the desired quiet zone region over space and frequency, and e_s is the error signal at a field point and P_{pbs} is the broad-band diffuse primary field at the field points. This approach ensures that the area of the 10dB quiet zone inside the desired quiet zone region over space and frequency is maximized.

From Equation (12) and (18), Equation (36) can be written as follows.

$$\begin{array}{l} \text{Maximizing} \quad A \\ \text{Subject to} \\ \left\| 10\log_{10} \dfrac{\left| P_{pbs} - P_{pb} W_1 \frac{A_1}{r_1(x,y)} e^{-j2\pi f r_1(x,y)/c} - P_{pb} W_2 \frac{A_2}{r_2(x,y)} e^{-j2\pi f r_2(x,y)/c} \right|^2}{\left| \sum_{f_{bn}=fl}^{fh} \sum_{K=1}^{K\max} \sum_{L=1}^{L\max} (a_{KL}(f_{bn}) + j b_{KL}(f_{bn})) \sin\theta_K \exp\left(j \frac{2\pi}{c} f_{bn}(x \sin\theta_K \cos\varphi_L + y \sin\theta_K \sin\varphi_L)\right) \right|^2} \right\|_\infty \\ < \quad -10\text{dB inside the area } A, \\ \left\| W_1 B_1 \frac{A_{1o}}{r_{1o}(x,y)} e^{-j2\pi f r_{1o}(x,y)/c} + W_2 B_2 \frac{A_{2o}}{r_{2o}(x,y)} e^{-j2\pi f r_{2o}(x,y)/c} \right\|_\infty < 1 \\ \left\| \left(1 - W_1 \frac{A_1}{r_1(x,y)} e^{-j2\pi f r_1(x,y)/c} - W_2 \frac{A_2}{r_2(x,y)} e^{-j2\pi f r_2(x,y)/c}\right) D \right\|_\infty < 1 \end{array} \tag{37}$$

The optimal values of the filter coefficients W_1 and W_2 can be calculated using the function *fmincon*( ) in MATLAB. In the next section we evaluate the performance of the quiet zones in broad-band diffuse fields obtained using the proposed method.

4. **Simulation Results.** This section presents the simulation results for quiet zones in broadband diffuse fields using two-channel and three-channel systems in the effort to maximize the area of the 10dB quiet zone. The quiet zones are also compared with those obtained by using the H_2 pressure minimization strategy [18]. The primary field is a broad-band diffuse field. Two and three monopoles are used as the secondary fields in this study. A microphone is placed at the $(0.1\text{m}, 0)$ point, i.e., 10cm from the secondary monopole source. The novel method of maximizing the area of the 10dB quiet zone is

used to design the quiet zone in the broadband diffuse fields. The control filters with 64 coefficients are used. A series of simulations are performed to analyze the quiet zones in the broadband diffuse fields.

In the first simulation, two secondary monopoles are located at the origin and $(-0.05\text{m}, 0)$ point, controlling the broadband diffuse fields. A 10dB quiet zone over space and frequency without constraints on amplification and robust stability is computed using the area maximization of the 10dB quiet zone and compared with a quiet zone created by using H_2 control [18]. Figure 6 shows the 10dB reduction contour line over space and frequency for the area maximization of the 10dB quiet zone (solid line) inside a desired quiet zone area represented by the rectangular frame. Also shown is the 10dB reduction contour line for the H_2 control strategy (dash-dot line). Figure 6 shows that the zone of quiet created by using area maximization is larger than that created by the H_2 control strategy over this carefully selected area. This is because the two secondary monopoles obtained with the area maximization method attempt to maximize the area of the 10dB quiet zone. Therefore, the amplitude of the secondary field is as close as possible to the 10dB reduction amplitude of the primary field with the opposite phase over the complete desired quiet zone. This is in contrast to the H_2 control strategy, where the sum of the squared acoustic pressure over space and frequency is minimized.

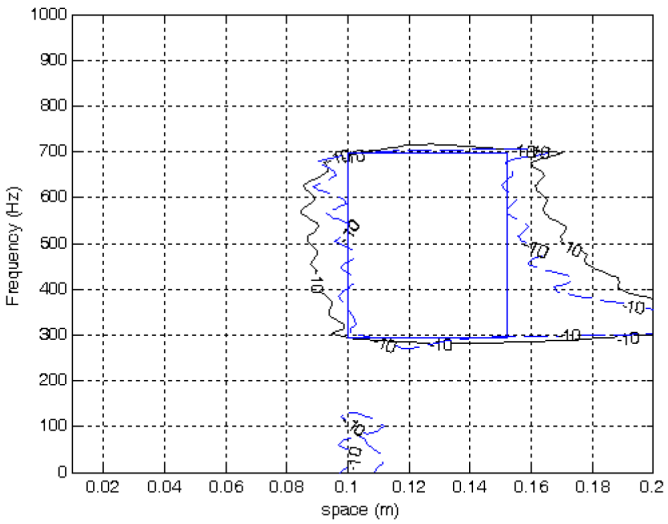

FIGURE 6. The 10dB reduction contour over space and frequency for the two-channel system with two FIR filters without constraints maximizes the area of the 10dB quiet zone at a desired quiet zone, as represented by a bold rectangular frame using area maximization strategy (solid line), and minimizes the acoustic pressure at an area, as represented by a bold rectangular frame (dash-dot line)

Figure 7 shows the attenuation contour over space and frequency without constraints on amplification and robust stability for the two-channel system with area maximization of the 10dB quiet zone. The secondary monopoles are located at the origin and $(-0.05\text{m}, 0)$ point, and the desired quiet zone area is the region enclosed in the rectangle. From the figure, we can observe that a high attenuation is achieved in the desired region. It can also be noted that the shape of the high-attenuation area is similar to that of the desired quiet zone area. This is because two monopoles can generate complicated secondary fields. Thus, good performance was obtained over the desired quiet zone area. A high amplification also appears at high-frequency regions and at the region close to the secondary monopoles.

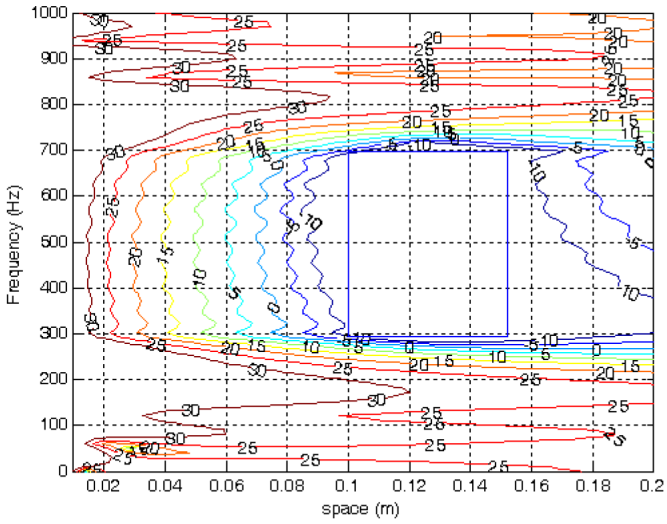

FIGURE 7. Attenuation contour in decibels as a function of space and frequency using the area maximization for the two-channel system with two FIR filters without constraints

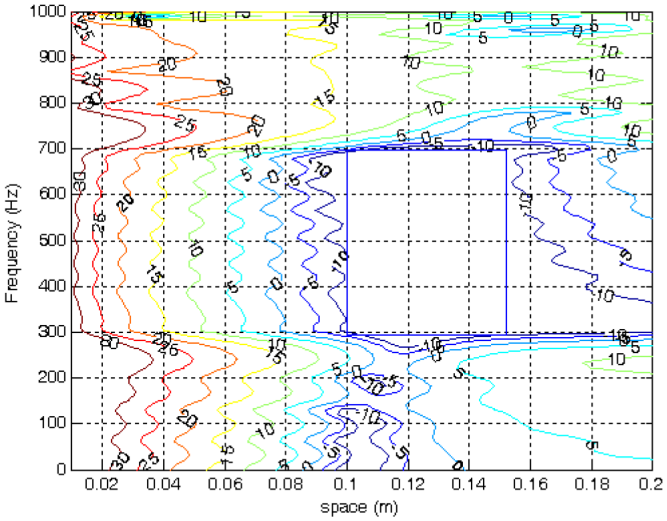

FIGURE 8. Attenuation in decibels as a function of space and frequency using area maximization for the two-channel system with two FIR filters and with constraints on amplification not exceeding 15dB at the spatial axis from $r = 0.1$m to $r = 0.2$m for all frequencies and constraints on robust stability with $B_1 = B_2 = 0.3$

In the second simulation, constraints on amplification and robust stability are added to the optimization process to prevent high amplification and instability. Figure 8 shows the attenuation contour over space and frequency using area maximization for the two-channel system with an amplification constraint not exceeding 15dB at the spatial axis from $r = 0.1$m to $r = 0.2$m for all frequencies and a constraint on robust stability with $B_1 = B_2 = 0.3$. We can see that the attenuation area becomes smaller than that without amplification and robust stability constraints.

In the third simulation three secondary monopoles are used to control the broadband disturbance. The attenuation contour over space and frequency using the area maximization for a three-channel system without constraints is shown in Figure 9. The secondary monopoles are located at the origin, $(-0.03\text{m}, 0)$ and $(0.03\text{m}, 0)$ points and the desired

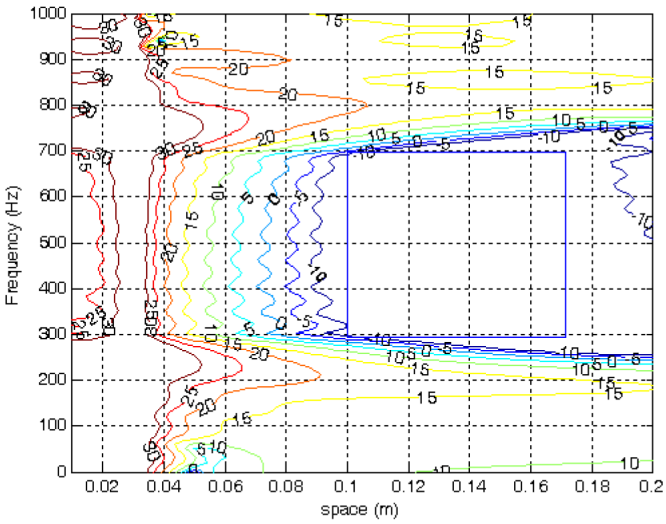

FIGURE 9. Attenuation in decibels as a function of space and frequency using area maximization for a three-channel system with FIR filters without constraints

quiet zone region is larger than that in the two-channel system as shown in Figure 7. From the figure, we can see that high attenuation is achieved in the desired region which is larger than that in the case of the system with two secondary monopoles as shown in Figure 7. It can also be seen that the shape of the high attenuation area is similar to that of the desired quiet zone region. This is because three secondary monopoles created more complicated secondary fields than those in the system with two secondary monopoles. Thus, better performance over the desired quiet zone region was obtained as expected. High amplification also appears at high frequencies and at the region close to the secondary monopoles.

In the fourth simulation the effect of the different shapes of the desired quiet zone on the size of the attenuation contours with three secondary monopoles was also investigated in this study. Figures 10(a) and 10(b) show the attenuation contours over space and frequency for three secondary monopoles without constraints on robust stability and amplification for the desired quiet zone with different shapes. It can be seen that the shape of the 10dB attenuation contour changes with the shape of the desired quiet zone. In Figure 10(a), the 10dB attenuation contour has a narrow shape in the frequency axis and a longer shape in the space axis which is similar to the shape of the desired quiet zone. When the shape of the desired quiet zone becomes narrower in space axis and longer in frequency axis, the 10dB attenuation contour tends to extend its size in the frequency axis as shown in Figure 10(b). Therefore, the shape of the 10dB attenuation contour can be designed using the method presented in the study.

5. **Experiments.** This section describes the experiment to validate the simulation results of the quiet zones in broad-band diffuse fields using the area maximization of the 10dB quiet zone. The excitation frequency range of 250-750Hz was chosen for the primary source. Figure 11 shows the experimental set-up used in the measurements. The secondary sources are two 110mm diameter loudspeakers placed separately. The grid has a 15mm pitch made of a brass rod with a diameter of 3mm. The dimensions of the grid are 600×600mm. The electret's microphones are located at the corresponding nodes of the grid. The size of the room where the experiment was performed is $10\text{m} \times 8\text{m} \times 4\text{m}$ and it is

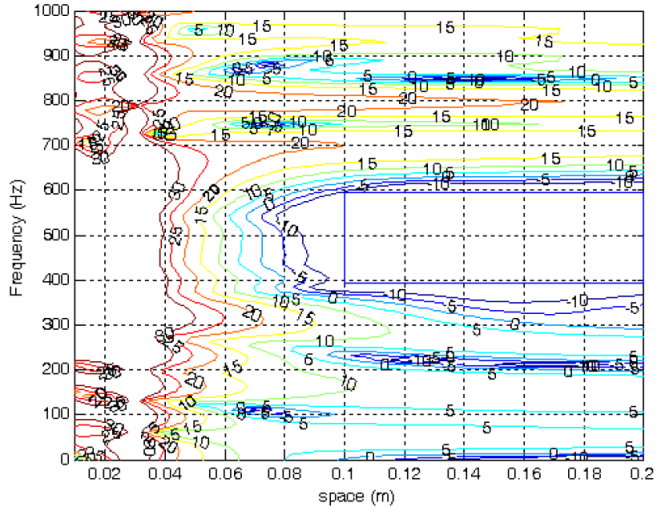

(a)

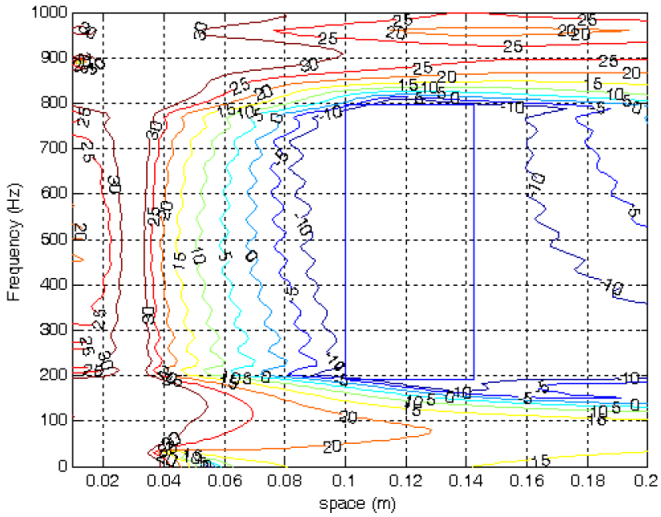

(b)

FIGURE 10. Attenuation in decibels as a function of space and frequency using area maximization for a three-channel system with FIR filters without constraints on the different shapes of the desired quiet zone represented by a rectangular frame. (a) The rectangular frame is narrower in the frequency axis direction and longer in the space axis direction. (b) The rectangular frame is narrower in the space axis direction and longer in the frequency axis direction.

a normal room. The primary source was located 6m away from the microphone grid. The primary field can be assumed to be a slightly diffuse field due to the effect of reflection.

The primary and secondary sources were connected to an FFT analyzer whose output can be selected with a switch that allows the signal to be fed to the primary source or to the secondary source. The reference signal necessary for the acquisition system to calculate the relative amplitude and phase of the complex acoustic pressure at the microphone positions was also connected to an FFT analyzer. All the microphones were connected to an electronic multiplexer which sequentially selects three microphone signals which were filtered by the low pass filter and then acquired by the Analogue Unit Interface (AUI). The sampling frequency was 2,000Hz and 4,000 samples are acquired for every microphone.

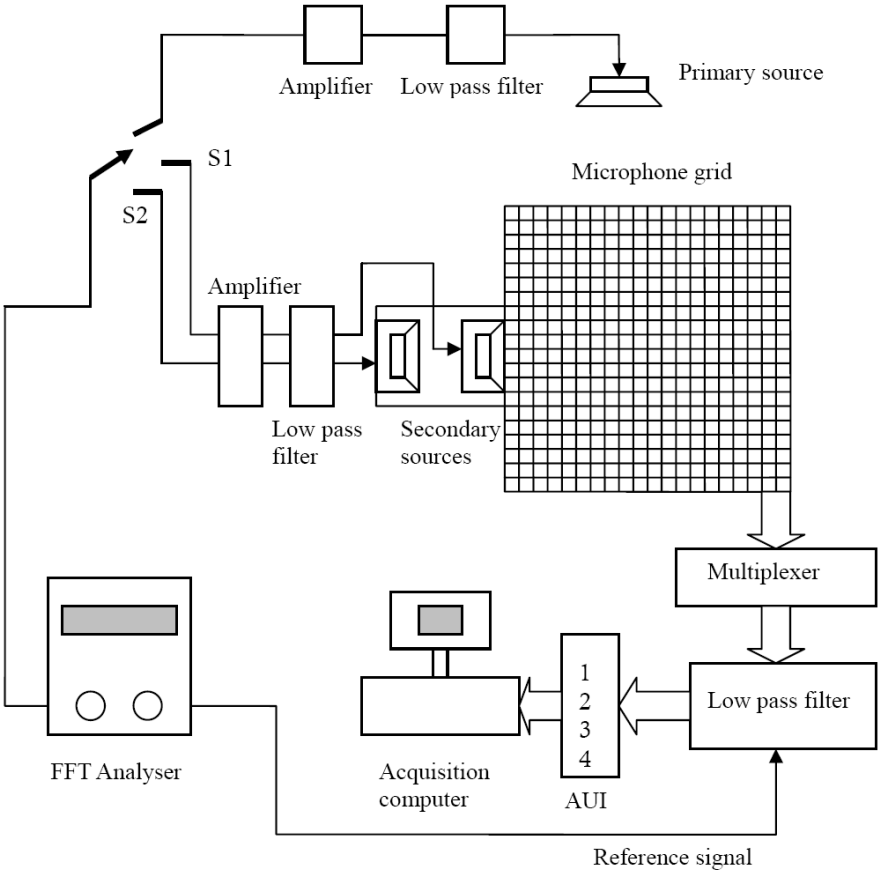

FIGURE 11. Configuration of the experimental set-up

The input signal to the AUI through channel 4 was taken as a reference to calculate the relative amplitude and phase of all the signals measured by the microphones on the grid. The calculation of the relative amplitude and phase of the pressure signals was carried out by the computer by Fourier transforming the four input signals and calculating the amplitude and phase of the microphone signals at the excitation frequency with respect to the reference signal. After a complete cycle a matrix of the complex pressure values at all the grid points was therefore obtained.

At this stage, the quiet zones created by two secondary loudspeakers were investigated through experiments with primary fields at the frequency range of 250-750Hz in the room described above. The primary fields were measured first, and the transfer functions between the secondary loudspeakers and all the microphones on the microphone grid were then measured. The primary field and transfer functions were then taken to calculate the optimal filter coefficients as in Equation (37). The zone of quiet was calculated as the ratio of the total (controlled) squared pressure and the primary squared pressure. Figure 12(a) shows the 10dB zone of quiet created by using the area maximization of the 10dB quiet zone through computer simulations. Figure 12(b) shows results equivalent to those seen as in Figure 12(a) through experiments. This shows that the shapes and sizes of the 10dB quiet zones are similar in the computer simulations and experiments. In Figure 12(a), monopole sources were used as secondary sources in the simulations. In Figure 12(b), however, loudspeakers were used as secondary sources in the experiments. Although monopole sources are not an accurate model for loudspeakers, this method simplifies the secondary source modeling and assists in comparison between simulations and experiments.

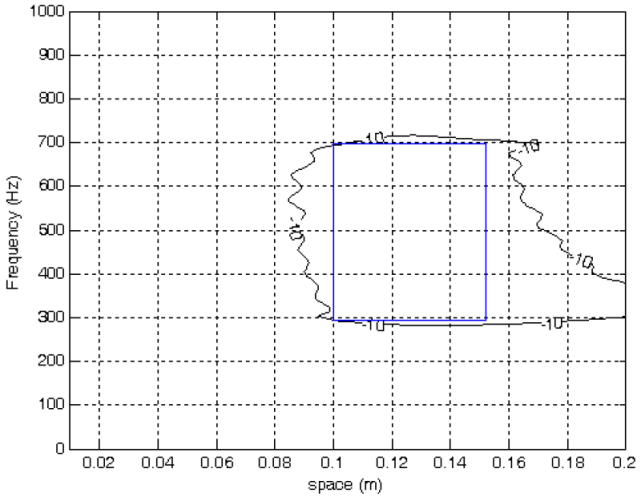

(a)

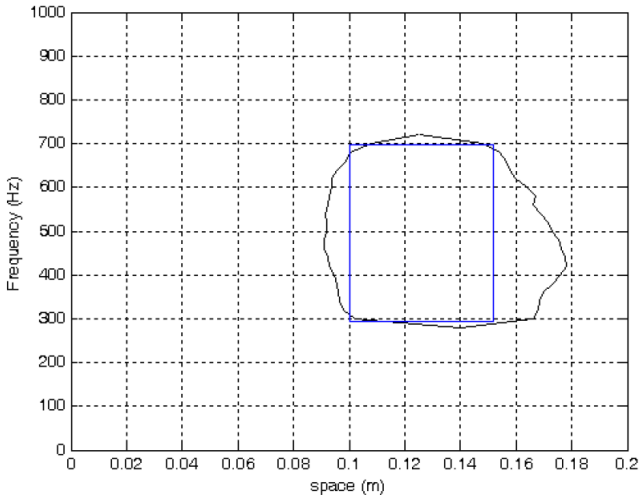

(b)

FIGURE 12. The 10dB reduction contour of the zones of quiet created by two secondary sources located at positions $(0, 0)$ and $(-0.05, 0)$ using the area maximization of the 10dB quiet zone. (a) Computer simulations. (b) Experiments.

6. **Conclusions.** A novel method involving the area maximization of the 10dB quiet zone to design quiet zones in broad-band diffuse fields has been presented and the quiet zone analysis using two-channel and three-channel systems has also been investigated through computer simulations and experiments. The 10dB quiet zone was maximized at the specified region over space and frequency. Constraints on amplification and robust stability were also included in the design process. The results showed that a good attenuation in the desired quiet zone over space and frequency could be achieved using a two-channel system. However, better performance was achieved using a three-channel system. When limits on amplification and robust stability were introduced, the performance began to degrade. It has also been shown that the shape of the quiet zone can be controlled by using the proposed method. Moreover, an experiment to validate the simulation results of the quiet zones in broad-band diffuse fields using the proposed method was also carried out. The results showed that the shapes and sizes of 10dB quiet zones are similar in both computer simulations and experiments.

Acknowledgment. This work is partially supported by the National Science Council of Taiwan, under project number NSC-100-2221-E-018-010. The author also gratefully acknowledges the helpful comments and suggestions of the reviewers, which have improved the presentation.

REFERENCES

[1] P. A. Nelson and S. J. Elliott, *Active Control of Sound*, Academic Publishers, London, 1992.
[2] S. Ishimitsu and N. Shibatani, Phase corrected filtered-error LMS algorithm and its application to the active control of ship interior noise, *International Journal of Innovative Computing, Information and Control*, vol.4, no.12, pp.3207-3217, 2008.
[3] P. A. Nelson and S. J. Elliott, The minimum power output of a pair of free field monopole sources, *Journal of Sound and Vibration*, vol.105, pp.173-178, 1986.
[4] M. Pawelczyk, Adaptive noise control algorithms for active headrest system, *Control Engineering Practice*, vol.12, pp.1101-1112, 2004.
[5] C. F. Ross, *Active Control of Sound*, Ph.D. Thesis, University of Cambridge, 1980.
[6] P. Joseph, *Active Control of High Frequency Enclosed Sound Fields*, Ph.D. Thesis, University of Southampton, 1990.
[7] P. Joseph, S. J. Elliott and P. A. Nelson, Nearfield zones of quiet, *Journal of Sound and Vibration*, vol.172, pp.605-627, 1994.
[8] A. David and S. J. Elliott, Numerical studies of actively generated quiet zones, *Applied Acoustics*, vol.41, pp.63-79, 1994.
[9] M. Miyoshi, J. Shimizu and N. Koizumi, On arrangements of noise controlled points for producing larger quiet zones with multi-point active noise control, *Inter-Noise*, pp.1229-1304, 1994.
[10] J. Guo and J. Pan, Analysis of active noise control in a free field, *Proc. of Active*, pp.649-660, 1995.
[11] J. Guo, J. Pan and C. Bao, Actively created quiet zones by multiple control sources in free space, *J. Acoust. Soc. Am.*, vol.101, pp.1492-1501, 1997.
[12] S. Ise, Theory of acoustic impedance control for active noise control, *Inter-Noise*, pp.1090-1095, 1994.
[13] J. Garcia-Bonito, S. J. Elliott and C. C. Boucher, A novel secondary source for a local active noise control system, *Active*, pp.405-418, 1997.
[14] S. J. Elliott and J. Garcia-Bonito, Active cancellation of pressure and pressure gradient in a diffuse sound field, *Journal of Sound and Vibration*, vol.186, pp.696-704, 1995.
[15] B. Rafaely, Spatial-temporal correlation of a diffuse sound field, *J. Acoust. Soc. Am.*, vol.107, no.6, pp.3254-3258, 2000.
[16] I. Chun, B. Rafaely and P. Joseph, Experimental investigation of spatial correlation of broadband diffuse sound fields, *J. Acoust. Soc. Am.*, vol.113, no.4, pp.1995-1998, 2003.
[17] X. Y. Zeng, An improved broad-spectrum room acoustics model including diffuse reflections, *Applied Acoustics*, vol.66, pp.1309-1319, 2005.
[18] W. K. Tseng, Quiet zone design in broadband diffuse fields, *International MultiConference of Engineers and Computer Scientists*, pp.1280-1285, 2009.
[19] S. Skogestad and I. Postlethwaite, *Multivariable Feedback Control*, John Wiley and Sons, Chichester, UK, 1996.
[20] M. Morari and E. Zafiriou, *Robust Process Control*, Prentice-Hall, NJ, 1989.
[21] R. Fletcher, *Practical Methods of Optimization*, John Wiley & Sons, 1987.
[22] G. R. Walsh, *Methods of Optimization*, John Wiley & Sons, 1975.
[23] H. W. Kuhn and A. W. Tucker, Nonlinear programming, *Proc. of the 2nd Berkeley Symposium on Mathematical Statistics and Probability*, pp.481-492, 1951.
[24] S. Boyd and L. Vandenberghe, *Convex Optimization*, Cambridge University Press, 2004.
[25] A. Grace, *Matlab Optimization Toolbox*, The Math Works Inc., 1995.